Ab initio Green-function formulation of the transfer matrix: Application to complex band structures

D. Wortmann,[1,*] H. Ishida,[2] and S. Blügel[3]
[1]*Institut für Festkörperforschung, Forschungszentrum Jülich, 52425 Jülich, Germany*
[2]*College of Humanities and Sciences, Nihon University, Sakura-josui, Tokyo 156, Japan*
[3]*Fachbereich Physik, Universität Osnabrück, 49069 Osnabrück, Germany*
(Received 8 October 2001; published 29 March 2002)

A method for the first-principles calculation of the transfer matrix is presented. The method is based on a Green-function formulation and allows one to relate the wave functions and their derivatives on boundaries at opposite sides of a film or junction of finite thickness. Both the underlying theory and an actual implementation in the full-potential linearized augmented plane wave method are described. Currently the embedding method is used to evaluate the Green-function matrix elements and in turn we show that the transfer matrix can be used to construct the embedding potential. Some possible applications of the transfer-matrix method such as the calculations of the complex band structure or the calculation of the transmission and reflection coefficients for ballistic transport are discussed. As a first example, complex band structures of Cu, Fe, and Si are presented.

DOI: 10.1103/PhysRevB.65.165103 PACS number(s): 71.15.Ap, 73.40.−c, 72.10.−d, 73.20.At

I. INTRODUCTION

An electron propagating through a crystal towards an interface can either reflect or transmit. This rather simple statement is at the heart of fields such as nanoelectronics, magnetoelectronics, spin electronics, or molecular electronics—areas of great importance for future technology. Understanding the transport properties on the basis of the underlying electronic structure is a key issue. On the other hand, over the past decades, the core of methods developed to perform *ab initio* electronic structure calculations based on density functional theory focussed on finding eigenstates for electrons in increasingly more complex material systems. These eigenstates are usually calculated within some slab or supercell geometry with periodic boundary conditions, are used to calculate the total energy of the system or forces exerted on the atoms. In the field of transport, however, in particular ballistic transport, one has to consider a scattering problem. In the asymptotic region, i.e., in the interior of the electrodes on both sides of the interface, transmitted and reflected electron waves are expressed as the superposition of generalized Bloch states. The generalized Bloch states include the propagating Bloch waves as well as evanescent states that decay exponentially. The amplitudes of these waves are determined such that the total wavefunction connects smoothly to the solutions of the Schrödinger equation in the interface region.

In the past a number of methods have been developed which address the problem of calculating the transmission of ballistic electrons through interfaces. Among these are methods which directly integrate the Schrödinger equation across the interface and construct a solution of the entire problem by matching the solutions at some boundary surface to the bulk solutions.[1–5] To avoid numerical instabilities in integrating the Schrödinger equation, Wachutka[6] and Stiles and Hamann[7,8] developed methods in which the initial value problem is translated into a boundary value problem. Lang[9] invented a method to calculate the conductance for an isolated molecule located between two semi-infinite jellium electrodes recently applied by Di Ventra *et al.*[10,11] Van Hoof *et al.*[12] employed the embedding method of Inglesfield[13] to calculate the transmission matrices in magnetic interfaces. Other schemes reformulated the Landauer-Büttiker[14] formula of ballistic transport in terms of a description based on single-electron Green functions. They are further classified into simple phenomenological models,[15] tight-binding (TB) models,[16–20] and those using the more realistic TB-LMTO (Refs. 21,22) or KKR methods.[23,24] Currently also methods[25,26] are being explored which derive the ballistic conductance from calculations in supercell geometry.

In the present work, we will present a general method which can be applied to a wide variety of problems. For example it can be used to calculate the complex bandstructure of bulk crystals, ballistic transport properties of interfaces, and the electronic structure of semi-infinite surfaces. It is based on a transfer matrix for one-electron wave functions which is calculated using a Green function in the linearized augmented plane wave (LAPW) basis. The method should therefore inherit from the full-potential LAPW (FLAPW) method the generality in the choice of systems and the accuracy in the description of the underlying electronic structure which was often missing in previous approaches. As a proof of principle, we calculate in this paper the complex band structures of bulk Cu, ferromagnetic Fe, and Si. The complex band structure is a concept which is fundamental for the description of the scattering at interfaces. It has recently received much attention as Mavropoulos *et al.*[27] has shown that it provides a very good understanding of the spin-dependent tunneling in magnetic tunnel junctions. The choice of systems was motivated in order to compare our results with those available in the literature as well as to demonstrate the wide variety of systems which can be studied ranging from semiconductors to ferromagnets. The good agreement with previous results opens the perspective to treat complex multicomponent systems in the near future.

The paper is organized as follows. In Sec. II we will give

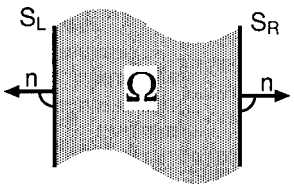

FIG. 1. Setup used to calculate the transfer matrix. The region of interest is a slab Ω between the two boundaries S_L and S_R. Ω is infinite in two dimensions and of finite size normal to the boundaries. The surface normals indicated by arrows are assumed to point outwards.

a general outline of our approach. The transfer matrix is defined and the relation to a specific Green function is presented leaving a more general expression to the Appendix. In Sec. III we discuss two possible applications in more detail, the calculation of the complex bandstructure and of transmission coefficients. In Sec. IV we show how the embedding method is employed to construct the adequate Green function. Details specific to the actual implementation in the FLAPW method is discussed in Sec. V. Section VI contains first numerical results. Finally, we summarize the main results of this paper and give a short outlook on possible future extensions. Unless stated otherwise we use the Hartree atomic units with $e=m=\hbar=1$ throughout this paper.

II. TRANSFER MATRIX

We start with defining a region of space Ω which has the shape of a slab (see Fig. 1), i.e., we assume that Ω is infinite in two dimensions and of finite size in the third dimension. To get an idea we have in mind, the slab could consist of a single layer of atoms of bulk material with two-dimensional translation symmetry, called a monolayer, or of a few monolayers, forming a heterostructure or describing an interface between two semi-infinite crystals. The boundary surface of the slab volume Ω is divided into two parts: the left boundary S_L and the right one S_R. Throughout the paper we will use the indices L and R to denote quantities defined on S_L and S_R, respectively, and index b to refer to either L or R. S without any index refers to both S_L and S_R. Given a local and spin independent potential energy defined in Ω and on S, $V(\vec{r})$, we consider solutions of the Schrödinger equation corresponding to this potential. Since the Schrödinger equation is a second order differential equation, its solution $\psi(\vec{r})$ in Ω with complex energy $Z=\epsilon+i\delta$ is completely determined by specifying the value $\psi(\vec{r}_b)$ and its local normal derivative $\partial_n\psi_b=\partial_n\psi(\vec{r}_b)=(\partial/\partial n)\psi(\vec{r}_b)$, on one of the boundary surfaces S_b. As indicated in Fig. 1, the positive surface normal is chosen to point outwards with respect to the region Ω. To simplify the notation, we define a vector of the boundary values

$$\Psi_b=\begin{pmatrix}\psi(\vec{r}_b)\\ \partial_n\psi(\vec{r}_b)\end{pmatrix}. \tag{1}$$

The key quantity of the method presented in this paper is the transfer matrix T, called the T matrix hereafter. It maps the left boundary values of a solution of the Schrödinger equation onto the right ones:

$$\Psi_R=T\Psi_L. \tag{2}$$

Now, we will show that the T matrix can be expressed in terms of the Green function defined in Ω

$$(\hat{H}-Z)G(\vec{r},\vec{r}\,';Z)=-\delta(\vec{r}-\vec{r}\,'), \tag{3}$$

where $\hat{H}$ is the usual Hamiltonian consisting of the potential and kinetic energy terms. Applying Green's theorem to the homogeneous and inhomogeneous Schrödinger equation, the wave function $\psi(\vec{r})$ in region Ω including the boundary surface S can be expressed by the Green function $G(\vec{r},\vec{r}\,';Z)$ (see, for example, Ref. 13),

$$\psi(\vec{r})=-\frac{1}{2}\int_{S_L+S_R}[G(\vec{r},\vec{r}_b)\partial_n\psi(\vec{r}_b) - \partial_n G(\vec{r},\vec{r}_b)\psi(\vec{r}_b)]d^2\vec{r}_b, \tag{4}$$

where the energy dependence of the Green function has been omitted for simplicity. It should be noted that $\psi(\vec{r})$ may fulfill a different boundary condition on S than the Green function $G(\vec{r},\vec{r}\,')$. By placing $\vec{r}$ in Eq. (4) either on S_L or on S_R, one obtains a set of linear equations relating ψ_b and $\partial_n\psi_b$. Comparing these linear equations with the definition of the T matrix in Eq. (2), one obtains an expression for the T matrix in terms of the Green function and its surface derivative. A particularly simple form is obtained by choosing a Green function which satisfies the von Neumann boundary condition of vanishing normal derivative on S:

$$\frac{\partial}{\partial n}G(\vec{r},\vec{r}_b;Z)=0 \quad \text{for} \quad \vec{r}\neq\vec{r}_b. \tag{5}$$

In this case one can derive a simple matrix expression for the T matrix in terms of surface Green functions,

$$T=\begin{pmatrix} G_{RR}G_{LR}^{-1} & -\frac{1}{2}G_{RL}+\frac{1}{2}G_{RR}G_{LR}^{-1}G_{LL}\\ -2G_{LR}^{-1} & -G_{LR}^{-1}G_{LL}\end{pmatrix}, \tag{6}$$

where the surface Green functions G_{LL}, G_{LR}, G_{RL}, and G_{RR} are defined by placing $\vec{r}$ and $\vec{r}\,'$ onto the boundaries S_b and $S_{b'}$, respectively. For example $G_{LR}(Z)=G(\vec{r}_L,\vec{r}_R;Z)$, with the first argument of the Green function placed on S_L and the second on S_R. Systems exhibiting collinear magnetism are diagonal in spin space and the formalism above applies to both spin-up and -down states independently.

Let us consider a one-dimensional free-electron system as a simplest application of Eq. (6). Assuming that Ω occupies the interval $0\leqslant z\leqslant d$, the Green function satisfying Eq. (5) is given by $G(z,z')=2\cos(kz_1)\cos[l(d-z_2)]/[k\sin(kd)]$, where $k=\sqrt{2Z}$, and z_1 and z_2 denote the smaller and larger of z and z', respectively. Thus, we have $G_{LL}=G_{RR}$

$=2\cos(kd)/[k\sin(kd)]$ and $G_{LR}=G_{RL}=2/[k\sin(kd)]$. Substituting these in Eq. (6), one obtains a well-known expression found in elementary text books

$$T=\begin{pmatrix} \cos(kd) & -\sin(kd)/k \\ -k\sin(kd) & -\cos(kd) \end{pmatrix}. \tag{7}$$

Even though the formulation of the T matrix in terms of a Green function with vanishing normal derivative on S is simple, it is not compulsory to impose this boundary condition. The full expression for T taking also nonzero normal derivatives of the Green function into account can be found in the Appendix. To avoid misunderstandings, we would like to stress that the Green function with the von Neumann boundary condition is not necessarily suitable to calculate other quantities. For example the density of states given by the imaginary part of the Green function $n(\vec{r};\epsilon) = -2/\pi \,\mathrm{Im}\, G(\vec{r},\vec{r};\epsilon+i\delta)$ [where δ is an infinitesimal imaginary energy], corresponds to a density of states of an isolated slab with von Neumann boundary condition imposed, which is of little use. In particular, if Ω is part of a bulk system, the density of states of this system can only be calculated from a Green function which fulfills boundary conditions consistent with the bulk periodicity.

Before describing possible applications of the theory, we shortly want to compare our approach with existing methods. At first glance our method may appear similar to real-space methods such as those in Refs. 1,2. However, one important difference is that we do not obtain the transfer matrix by solving an initial value problem in which one chooses boundary values only at one surface and integrates the Schrödinger equation on a real space grid to obtain the values on the opposite side. Because of the existence of the exponentially increasing solutions of the Schrödinger equation such an approach is intrinsically unstable. Furthermore, so far the application of such methods has been restricted to local pseudopotentials and extensions to the nonlocal pseudopotentials or an all-electron description is very difficult. In our calculation of the T matrix by Eq. (6) both boundaries are treated on the same footing. A further point we want to mention is the difference between our definition of the transfer matrix and the one used for example by van Hoof *et al.*[12] While van Hoof *et al.* use an additional plane-wave basis outside region Ω, i.e., to the left of S_L and to the right of S_R, to define a transfer matrix which operates on states given in this basis at the boundaries, our method treats the region Ω only and does not depend on any outside region. As an advantage, Eq. (6) can be applicable to any curved surface.

III. APPLICATIONS

Having obtained the T matrix one can calculate various quantities of which we will present two in more detail: the complex bandstructure and the calculation of transport properties.

A. Complex band structure

Most fundamental is the calculation of the complex band structure as it is the basis of further applications of the theory. Generally, the term complex band structure[28,29] refers to the so-called ''real bands'' consisting of the solutions $\epsilon(\vec{k})$ with real energy ϵ and in general complex Bloch vectors $\vec{k} = \vec{q} + i\vec{\kappa}$. In the bulk of a crystal, the translation symmetry requires that the Bloch vectors are purely real. But near a crystal surface or interface the wave function of complex $\vec{k}$ vector can match with wavefunctions in the crystal, and thus are describing evanescent surface, interface, or metal induced gap states. Although these states with complex $\vec{k}$ vectors occur only in systems with broken translation symmetry, their general properties can be derived from the bulk band structure of the material, if one formally allows complex $\vec{k}$ vectors to characterize the solutions of the Schrödinger equation for the bulk potential. This can be understood from the observation that the modification of the charge density and the potential due to the interface is confined in the vicinity of the interface and stretches at most over a few atomic layers. An evanescent wave, on the other hand, can extend over many layers far into the bulk crystal, and is therefore represented by solutions of the bulk Schrödinger equation, but for complex wave vectors.

We now assume that the region Ω is a principle layer of a bulk crystal with three-dimensional translation symmetry. The principle layer is a bulk unit that can generate the infinite three-dimensional bulk material upon application of translation-symmetry operations normal to the layer. For example, for a lattice with bcc or fcc crystal symmetry the principle layer is just a monolayer, or a plane of atoms. Thus, there exists a translation vector $\vec{d}$ between S_L and S_R, which is a lattice vector and one can exploit this translation symmetry by the generalized Bloch theorem. In contrast to the usual (propagating) Bloch states, in applying the generalized Bloch theorem one does not require the states to be normalizable in the whole space, i.e., one also allows solutions of the Schrödinger equation which decay exponentially. Since these decaying states grow exponentially in the opposite direction of the crystal, these solutions are not solutions of an infinite crystal. For any generalized Bloch state the following condition will hold between Ψ_L and Ψ_R:

$$\Psi_R=\begin{pmatrix} \psi(\vec{r}_L+\vec{d}) \\ \partial_n\psi(\vec{r}_L+\vec{d}) \end{pmatrix} = \exp(i\vec{k}\vec{d})\tilde{I}\Psi_L, \tag{8}$$

where the matrix $\tilde{I}=\left(\begin{smallmatrix}1 & 0\\ 0 & -1\end{smallmatrix}\right)$ was introduced to take the definition of the positive surface normal into consideration, which reverses its direction as $\vec{r}_b$ changes from S_L to S_R. Together with Eq. (2) one obtains an eigenvalue problem

$$\tilde{T}\Psi_L=\lambda\Psi_L, \tag{9}$$

where $\tilde{T}=\tilde{I}T$. The T matrix is a general complex matrix with complex eigenvalues $\lambda=\exp(i\vec{k}\vec{d})$ which determine the complex bandstructure of the system. We obtain the real bands

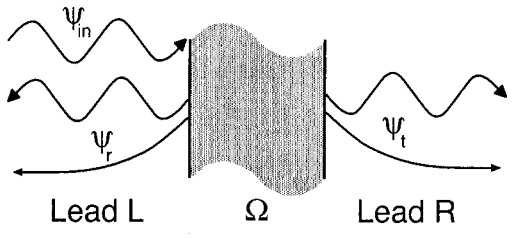

FIG. 2. Setup of the transport problem. The region Ω is sandwiched between two leads and contains all scattering potential. The potential in the leads to the left and the right is assumed to be bulklike. In the leads one incoming wave ψ_{in} and the reflected ψ_r and transmitted ψ_t generalized Bloch states of the complex band structure are sketched.

$\epsilon(\vec{k})$ in terms of $\vec{k}(\epsilon)$ by determining the T matrix $T(\epsilon)$ for a set of real energies ϵ and solving Eq. (9) for $\lambda(\epsilon)$.

At this point we would like to stress some important properties of the T matrix. As the solution of the Schrödinger equation is uniquely determined by the vector of the boundary values Ψ_L (or Ψ_R), the eigenvectors of the T matrix are linearly independent and the T matrix can be inverted. The inverse T matrix maps Ψ_R onto Ψ_L. For a real band, i.e., for an energy $Z=\epsilon$, it is easy to prove that $\epsilon(\vec{k})=\epsilon(-\vec{k})$ if the potential $V(\vec{r})$ is real and periodic.[29] Thus, the eigenvalues of the T matrix appear in pairs λ,λ' with $\lambda\lambda'=1$. In other words, for each eigenvalue λ of the eigenvalue spectrum of T corresponding to the generalized Bloch vector $\vec{k}$, there exists an inverse eigenvalue λ^{-1} corresponding to $-\vec{k}$. Therefore, the inverse T matrix T^{-1} has the same eigenvalue spectrum as T. This opens up an interesting aspect of the theory. The eigenvectors of T can be grouped into two sets. One set of eigenvectors corresponds to states which propagate to the left if $|\lambda|=1$ or decay to the left if $|\lambda|>1$. The other set contains eigenvectors describing states propagating to the right ($|\lambda|=1$) or decaying to the right $|\lambda|<1$. This classification of the eigenstates is important for the second application of the theory, which we discuss below: the calculation of transport properties.

In many applications one considers the scattering and transport of electrons at surfaces and interfaces. In this case, the corresponding surface or interface planes of the bulk crystal exhibits two-dimensional periodicity in the plane, and it is convenient to choose the planar component $\vec{k}_\parallel$ of $\vec{k}$ as real. As the Hamiltonian, the Green function, and the T matrix of the bulk crystal are diagonal in $\vec{k}_\parallel$, one can calculate the perpendicular component of $\vec{k}$, $k_z(\vec{k}_\parallel,\epsilon)$, as functions of $\vec{k}_\parallel$ and ϵ. For magnetic systems all quantities have an additional spin index.

B. Reflection and transmission coefficients

To define the problem, we will consider a ballistic electron approaching the left boundary surface from the left and being reflected in Ω or being transmitted into a lead to the right. As shown in Fig. 2 the total setup now consists of three regions, the left and right leads, and the region Ω. We assume that the scattering potential is confined within Ω, i.e., the potential in the leads is assumed to be the bulk crystal potential. The wave function corresponding to this scattering process is written as

$$\psi(\vec{r})=\begin{cases}\psi_{in}^{n}(\vec{r})+\sum_{m} r_{nm}\psi_{r}^{m}(\vec{r}), & \vec{r} \text{ left of } \Omega,\\ \sum_{n'} t_{nn'}\psi_{t}^{n'}(\vec{r}), & \vec{r} \text{ right of } \Omega,\end{cases} \tag{10}$$

where ψ_{in}^{n} denotes an incoming Bloch state n propagating to the right, the sum over m is carried out over all reflected states ψ_r propagating or decaying to the left into the left lead and the sum over n' is carried out over all transmitted states ψ_t propagating or decaying to the right into the right lead. According to the formulation of Landauer and Büttiker[14] for ballistic transport, the conductance G is obtained as

$$G=\frac{e^2}{h}\sum_{n}\sum_{n'}|t_{nn'}|^2. \tag{11}$$

The first and second sums in Eq. (11) are carried out over all the incoming and transmitted propagating states at the Fermi energy, respectively, and it is understood that they are normalized to have a unit current density. The reflection and transmission coefficients r_{nm} and $t_{nn'}$ can be determined matching the wave function across Ω, i.e., by the requirement that the total wave function is continuous and has continuous normal derivative at both boundaries of Ω.

The actual evaluation of the transmission coefficients for each incoming Bloch wave is generally a nontrivial problem. However, it can quite naturally be related to the transfer matrix, which gives the transfer-matrix method a high potential for later applications in areas of transport. The derivation of the transmission coefficient from the transfer matrix is straight forward. Placing $\vec{r}$ either on S_L or S_R one can rewrite Eq. (10) in terms of boundary values $\Psi_L=\Psi_{in}^{n}+\Sigma_m r_{nm}\Psi_r^m$ and $\Psi_R=\Sigma_{n'}t_{nn'}\Psi_t^{n'}$. Relating the boundary values by the T matrix in region Ω according to Eq. (2), we obtain the equation

$$\sum_{n'} t_{nn'}\Psi_t^{n'}=\tilde{T}\Psi_{in}^{n}+\sum_{m} r_{nm}\tilde{T}\Psi_r^m, \tag{12}$$

whose solution gives the transmission and reflection coefficients $t_{nn'}$ and r_{nm}.

IV. THE EMBEDDING METHOD

In the following we discuss the embedding method developed by Inglesfield[13] from the viewpoint of the present transfer-matrix method. At two different points one can make contact between the embedding method and the transfer-matrix method: (i) the embedding method can be used to obtain a Green function with the proper von Neumann boundary condition and (ii) the transfer-matrix method can be used to calculate the embedding potential.

In the embedding method, the Hamiltonian $\hat{H}_\Sigma$ contains

an additional term, which acts only at the boundary surface S, leading to the following form of the Schrödinger equation:

$$(\hat{H}_\Sigma - Z)\psi(\vec{r}) = 0, \tag{13}$$

where

$$\hat{H}_\Sigma \psi(\vec{r}) = \hat{H}\psi(\vec{r}) + \sum_{b=L,R} \frac{1}{2}\delta(n-n_b) \times \left(\frac{\partial \psi(\vec{r})}{\partial n} - 2\int_{S_b} V_\Sigma(\vec{r},\vec{r}_b;Z)\psi(\vec{r}_b)d^2\vec{r}_b \right), \tag{14}$$

where n is the surface normal coordinate and n_b specifies the position of S_b along n. In Eq. (14) the one-dimensional delta function ensures that the extra term acts only when $\vec{r}$ is on S_b. The extra term V_Σ is called the embedding potential and can be thought of as a generalized logarithmic derivative of the solution ψ at the boundary S_b of Ω:

$$\frac{\partial \psi(\vec{r}_b)}{\partial n} = 2\int_{S_b} V_\Sigma(\vec{r}_b,\vec{r}'_b;Z)\psi(\vec{r}'_b)d^2\vec{r}'_b. \tag{15}$$

In our scheme we use the embedding method only to obtain a Green function satisfying the von Neumann boundary condition on S_b. One realizes directly from Eq. (15) that this boundary condition is imposed if the embedding potential is set to zero, $V_\Sigma(\vec{r}_b,\vec{r}_{b'})=0$. If one furthermore solves in Eq. (13) the Green function

$$(\hat{H}_\Sigma - Z)G(\vec{r},\vec{r}\,';Z) = -\delta(\vec{r}-\vec{r}\,'), \tag{16}$$

instead of the wave function, one obtains the desired Green function with the von Neumann boundary condition Eq. (5). As pointed out in Ref. 30 the embedding method has the additional advantage of producing an accurate Green function especially when the arguments of the Green function are placed at the boundary surface, which is of crucial importance in our scheme. Since the present Green function corresponds to that of a finite slab, it has discrete poles on the real energy axis. Theoretically, the singularities related to those poles should be canceled such that the T matrix itself exhibits no singularity even on those energy values. It has turned out that this statement holds very well also numerically. So far we never had instability related to the poles of the Green function in our numerical calculations of the T matrix.

In the original paper by Inglesfield[13] and in subsequent applications to electronic structure calculations,[31–34] it was shown that the correct boundary condition of a small region embedded into a larger one can be incorporated by imposing a suitable embedding potential V_Σ. Formally, the embedding potential V_Σ is defined as a surface inverse of the Green function of the larger region, which has vanishing normal derivative on S_b, and which fulfills the outward boundary condition at the outer boundary of the larger region. However, this prescription is not suitable for practical calculations. In previous applications the embedding potential was generated either from a reflection matrix as obtained from a layer-KKR method[35,23] or by iterative schemes.[36,32] The former approach suffers from the muffin-tin approximation in the potential whereas the latter converges poorly when the imaginary part of the energy is too small. However, the boundary values obtained in a complex band structure calculation may be used to overcome this. The boundary values, i.e., the eigenvectors of T, do include both the values $\psi(\vec{r}_b)$ and the derivatives $\partial_n\psi(\vec{r}_b)$ of the wave function at the boundary surface S_b. Thus, by writing down Eq. (15) for all the generalized Bloch states propagating/decaying away from the surface and then inverting a matrix that comprises all of $\psi(\vec{r}_b)$ as its column vectors, one can obtain the embedding potential.

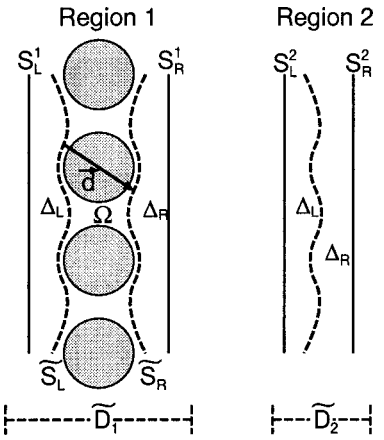

FIG. 3. Setup used to generate planar boundary surfaces. Two additional volumes are added (Δ_L and Δ_R) to Ω to obtain region 1. The second region consists only of the these additional volumes.

V. IMPLEMENTATION

The calculations in this paper are based on the FLAPW method, thus the Green function is expanded in LAPW's. In all APW based methods the space of the unit cell is partitioned into muffin-tin (MT) spheres around the atoms and an interstitial (int) region. Generally it is not possible to define a planar surface between adjacent monolayers which does not cut through muffin-tin spheres. Cutting through muffin-tin spheres introduces limitations in the numerical accuracy of the final results and should preferably be avoided. Using a curved surface, however, would make the formulation of the scheme extremely complicated. One option to overcome this difficulty may be the application of the augmented Fourier components method developed by Krasovskii *et al.*[37] in which the LAPW basis is substituted by a plane wave basis except for relatively small spheres surrounding the nuclei. However, his method cannot be applied, for example, to vicinal surfaces. In the present work, we use a setup as introduced in Refs. 36,38. As illustrated in Fig. 3 we add first auxiliary volumes Δ_L and Δ_R to the left and right of the curved boundary surfaces $\tilde{S}_L$ and $\tilde{S}_R$ of the slab Ω, respectively, until planar surfaces S_b^1 can be constructed. In addition, we use a second volume between the surfaces S_b^2 containing no muffin-tin spheres but only the regions Δ_L and Δ_R. They can be joined together at the curved surfaces $\tilde{S}_L$

and $\tilde{S}_R$, which are simply shifted by the lattice vector $\vec{d}$. We calculate the T matrix in both regions 1 and 2:

$$T_1 = T_{\Delta_R} T_\Omega T_{\Delta_L},$$

$$T_2 = T_{\Delta_R} T_{\Delta_L}. \tag{17}$$

From these T matrices we determine

$$T = T_1 T_2^{-1} = T_{\Delta_R} T_\Omega T_{\Delta_R}^{-1}. \tag{18}$$

The eigenvalues of the so-defined T matrix T and T_Ω are identical. The eigenvectors of T are given on S_R^2 and can be transfered by T_2^{-1} to S_L^2 which can be identified with S_L^1. In principle, the potential energy in auxiliary volumes Δ_L and Δ_R can be chosen arbitrarily. In the present work, we use the continuous extension of the FLAPW-interstitial potential. Its advantage is that the resultant potential becomes smooth throughout the entire regions 1 and 2, and that, as a result, one does not need to define the curved surfaces $\tilde{S}_b$ explicitly.

We expand the Green function with complex energy Z and the two-dimensional wave vector $\vec{k}_\parallel$ as

$$G_{\vec{k}_\parallel}(\vec{r},\vec{r}\,';Z) = \sum_{\vec{g},\vec{g}\,'} \phi_{\vec{k}_\parallel,\vec{g}}(\vec{r}) G_{\vec{k}_\parallel}(\vec{g},\vec{g}\,';Z) \phi^*_{\vec{k}_\parallel,\vec{g}\,'}(\vec{r}\,'), \tag{19}$$

where $\phi_{\vec{k}_\parallel,\vec{g}}(\vec{r})$ are defined in region 1 as

$$\phi_{\vec{k}_\parallel,\vec{g}}(\vec{r}) = \frac{1}{\sqrt{A}} \begin{cases} f_{g_z}(z) e^{i(\vec{k}_\parallel+\vec{g}_\parallel)\vec{r}_\parallel}, & \vec{r} \in \text{ int}, \\ \phi^{MT}_{\vec{k}_\parallel,\vec{g}}(\vec{r}), & \vec{r} \in \text{ MT}, \end{cases} \tag{20}$$

where A denotes a normalization area. In the muffin-tin spheres, the functions $\phi^{\mathrm{MT}}_{\vec{k}_\parallel,\vec{g}}(\vec{r})$ are linear combinations of radial functions $u_l(r)$ and their energy derivatives multiplied by spherical harmonics $Y_{lm}(\hat{r})$ given in a local coordinate system. They match the basis functions in the interstitial region at the muffin-tin spheres in value and slope. They could also be supplemented by local orbitals[39–41] or alternatively an APW+LO basis set could have been chosen as suggested by Sjöstedt *et al.*[42] The vectors $\vec{r} = (\vec{r}_\parallel, z)$ and $\vec{g} = (\vec{g}_\parallel, g_z)$ are split into a vector parallel to the surfaces and a z component perpendicular to the surface or interface, where $\vec{g}_\parallel$ are two-dimensional reciprocal lattice vectors corresponding to the lattice structure in the plane.

We implemented the formalism into two different FLAPW codes (e.g., see URL http://www.flapw.de), in which two forms of the z-dependent functions $f_{g_z}(z)$ have been used: $f_{g_z}(z) = (2/\tilde{D})^{1/2} \sin(g_z z)$ and $f_{g_z}(z) = (1/\tilde{D})^{1/2} \exp(i g_z z)$. Both implementations do lead to the same results. g_z is chosen to be

$$g_z = \frac{2\pi}{\tilde{D}} n, \tag{21}$$

where in the case of the sin basis, n is a half-integer number ranging from 0.5 to $n_{\max}+0.5$ ($n = 0.5, 1, 1.5, \ldots, n_{\max}+0.5$), and in the case of the exp basis, n is an integer with $-n_{\max} \leqslant n \leqslant n_{\max}$. The width $\tilde{D}$ is larger than the width of the region 1. This ensures that the basis set has sufficient variational freedom to describe the Green function at the boundaries of region 1. Using $N_\parallel$ two-dimensional vectors $g_\parallel$, this basis consists of $N_\parallel \times (2n_{\max}+1)$ functions. The basis functions in region 2 containing no muffin-tin spheres are constructed in the same way without any augmenting functions ϕ^{MT} in muffin-tin spheres and with $\tilde{D}$ larger than the width of $\Delta_L + \Delta_R$. Using the basis set, Eq. (16) turns into a matrix equation for the Green-function matrix $G(\vec{g},\vec{g}\,')$. The T matrix in Eq. (6) can be written in terms of the matrices of the surface Green functions

$$G_{bb'}(\vec{g}_\parallel,\vec{g}\,'_\parallel) = \frac{1}{A} \sum_{g_z g_z'} f_{g_z}(z_b) G(\vec{g},\vec{g}\,') f^*_{g_z'}(z_{b'}). \tag{22}$$

One should note that these matrices of the boundary surface Green functions $G_{bb'}$ are contractions of the total Green-function matrix over the basis functions describing the variational degrees of freedom normal to the surface S. These matrices $G_{bb'}$ are defined only in the two-dimensional basis and therefore are only of size $(N_\parallel \times N_\parallel)$. The T matrix is a $(2N_\parallel \times 2N_\parallel)$ matrix and the boundary values Ψ_b are vectors of dimension $2N_\parallel$. Some extra care has to be taken when the lattice vector $\vec{d}$ is not normal to the surface S, i.e., when the projection $\vec{d}_\parallel$ onto the surface S does not vanish. In this case an additional phase factor has to be included in the generalized Bloch condition and the final Eq. (9) is rewritten as

$$\sum_{\vec{g}'_\parallel, i'=1,2} e^{i\vec{g}_\parallel \vec{d}_\parallel} \tilde{T}(\vec{g}_\parallel, i; \vec{g}'_\parallel, i') \Psi_L(\vec{g}'_\parallel, i') = \lambda \Psi_L(\vec{g}_\parallel, i), \tag{23}$$

where $i=1$ denotes the value and $i=2$ the normal derivative component of $\tilde{T}$ and Ψ_L. Equation (23) is then solved for a set of $\vec{k}_\parallel$ points and energies ϵ, and in case of magnetic systems also for spin up and down states.

To ensure sufficiently accurate two-dimensional surface Green-function matrices $G_{bb'}$, the basis functions have been chosen such that the $\vec{g}$ vectors are taken out of a cylinder with radius $g_\parallel^{\max}$, $\{\vec{g} \,|\, |\vec{k}_\parallel + \vec{g}_\parallel| \leqslant g_\parallel^{\max}, g_z = (2\pi/\tilde{D})n\}$, and not from the standard sphere $\{\vec{g} \,|\, |\vec{k}+\vec{g}| \leqslant g_{3D}^{\max}\}$. Typical cutoffs in our calculations were $N_\parallel = 25$ $[(g_\parallel^{\max})^2 \approx 9\text{–}16$ Ry] two-dimensional plane waves and for each of these $2n_{\max} \approx 30$ basis functions in the z direction. This includes some unusually large $\vec{g}$ vectors in the plane wave basis set, which requires additional attention. Large $\vec{g}$ vectors correspond to high kinetic energy contributions to the interstitial part of the Hamiltonian matrix. To obtain a sphere representation of the basis function which is well matched at the sphere boundary to the plane waves and represents the kinetic energy contribution in the muffin-tin sphere with the same accuracy as in the interstitial region, we work with a high angular momen-

tum l_{max} cutoff for the sphere representation. In our calculations values of $l_{max} \approx 20-30$ had to be taken into account. However, as the basis functions with large $\vec{g}$ describe nearly free electrons, the high l_{max} cutoff is only necessary for the calculation of the overlap matrix and the matrix elements of the kinetic energy part of the Hamiltonian but not for the potential. Since these parts are diagonal in l and independent of the orbital number m, no significant additional computer time is consumed calculating these matrix elements to high cutoffs. Alternatively, the high l_{max} cutoff can be avoided using the modified basis set introduced by Soler and Williams.[43] However, this modification does not lead to any significant difference of the results while being computationally more demanding.

VI. RESULTS

As a first application of the method we present complex band structures of bulk Cu, Fe, and Si. For Cu and Fe the band structures include states along the [001] directions, i.e., states propagating or decaying perpendicular to a (001) oriented interface or surface, and for Si states in the [111] direction relevant for a (111) interface. The systems have been selected on grounds to show the flexibility of the method to cover semiconductors to ferromagnets, any interface or surface orientation, and to compare the results with existing ones in the literature. With respect to the latter, Cu and Si are particularly good cases as they have been studied extensively in the past. Fe is shown, because it is magnetic, and a magnetic complex band structure does not exist in the literature so far, although it is of increasing importance due to applications in the magnetoelectronics. In general our results are in excellent agreement with those published in the literature.

All calculations employ the density functional theory in the (spin-polarized) local density approximation (S)LDA. At first we determined a self-consistent bulk charge-density and potential at the experimental lattice constant of Cu ($a_{Cu}=3.61$ Å), Fe ($a_{Fe}=2.87$ Å), and Si ($a_{Si}=5.43$ Å). In a second step, we apply for the given potential the method described in the preceding sections which leads finally to the diagonalization of the T matrix for a selected $k_\parallel$ point of the two-dimensional Brillouin zone on a grid of real energies ϵ. The figures are produced using an equidistant energy grid of approximately 200 points.

In general, there is an infinite number of complex bands at any energy, but we only calculate a finite subset and show only the smallest wave vectors ($\kappa_z \lesssim 2$ a.u.$^{-1}$). Complex bands depart at right angle from the (real) q_z axis whenever there is a local minimum or maximum of the real band structure with respect to q_z and they can either extend in energy to $-\infty$, forming free-electron-like parabolic solutions or connect back to other extrema of the real band structure, forming closed loops. One can show analytically[29,44] that actually at all points where bands have zero slope, i.e., where bands are parabolic in $\vec{k}$ around a minimum or maximum, one finds another band crossing at right angle, which also has an extremum and opposite curvature.

In Figs. 4–6 we present the complex band structures, each

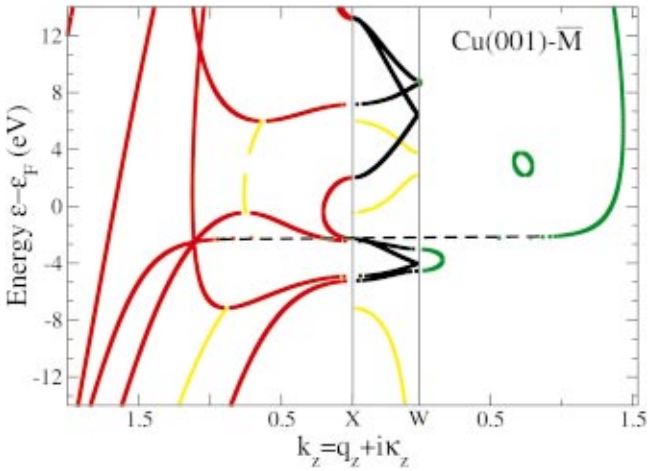

FIG. 4. (Color) Complex band structure of bulk Cu for $\vec{k}_\parallel$ chosen at the $\bar{M}$ point of the two-dimensional Brillouin zone of an (001) oriented interface plane. States for complex wave vectors ($\kappa_z \neq 0$) are shown in the left ($q_z=0$) and right ($q_z=1/2 \times \pi/a_{Cu}$) panel, the center panel shows bands with real wave vectors $\kappa_z=0$. κ_z is given in absolute units of a.u.$^{-1}=1.89$ Å^{-1}. For an explanation of the line colors, see text.

for one high-symmetry point in the two-dimensional Brillouin zone corresponding to the surface orientation under consideration. The (propagating) Bloch states, i.e., real bands with $\kappa_z=0$, are plotted as black dots in the center panel of each figure. The complex bandstructure includes all propagating Bloch states ($\vec{k}_\parallel, q_z$) along a line in a first bulk Brillouin zone which are projected onto the same $\vec{k}_\parallel$ point of the two-dimensional Brillouin zone. For the examples selected here, q_z are solutions along a high-symmetry line connecting two high-symmetry points with $q_z=0$ and $q_z \neq 0$, to which we refer to as the left and right high-symmetry point, respectively. The imaginary part κ_z of the wave vectors of the complex bands are plotted in the right- and left-hand panels of the figures in units of a.u.$^{-1}$. Red and green dots denote states corresponding to a wave vector q_z at the left ($q_z=0$) and right ($q_z \neq 0$) high-symmetry point, respectively. Complex bands with general k_z-values are indicated in the figures by two yellow dots corresponding to a projection of k_z onto the real and the imaginary plane. The real component q_z is plotted in the center panel together with the Bloch states with $\kappa_z=0$ and the imaginary component κ_z is shown in the left-hand panel together with the evanescent states with $q_z=0$.

A. Cu(001)-$\bar{M}$

Figure 4 shows the complex bandstructure of bulk Cu in the [001] direction at the $\bar{M}$ point $\vec{k}_\parallel=(1,1)\times\pi/a_{Cu}$ of the two-dimensional Brillouin zone. The q_z values follow the Z line in the bulk Brillouin zone, connecting the X point and the W point, left and right high-symmetry points, respectively. Figure 4 shows all features expected from the general considerations discussed above. At the high-symmetry points complex bands leave the real $\kappa_z=0$ plane. These bands either form loops connecting two of these maxima or they

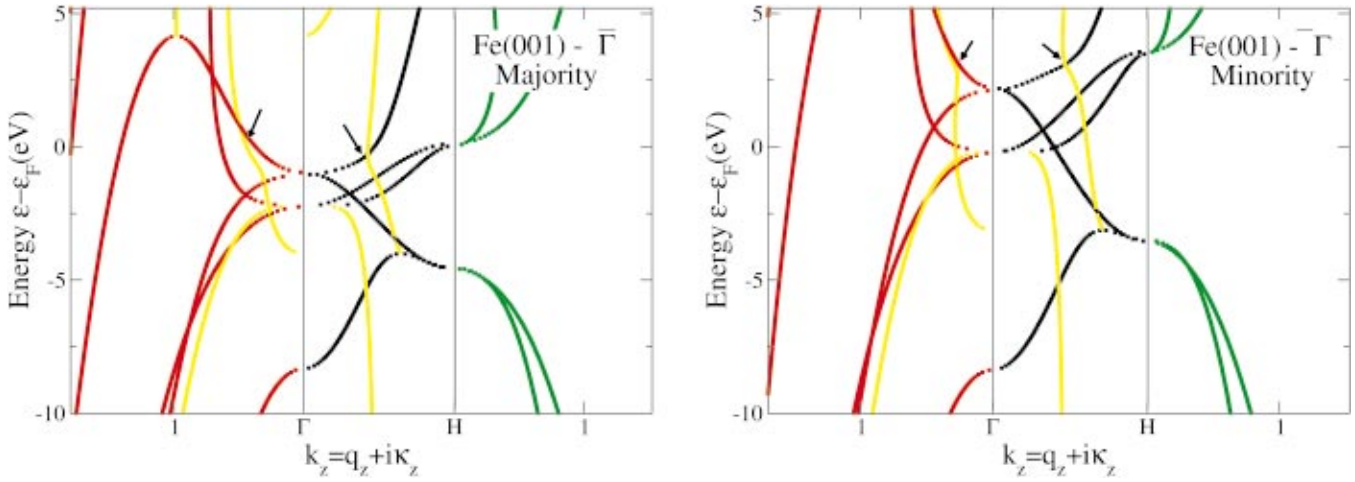

FIG. 5. (Color) Spin-dependent complex band structure of bcc Fe for $\vec{k}_{\|}$ chosen at the $\bar{\Gamma}$ point of the two-dimensional Brillouin zone of an (001) oriented interface plane. Left (right) figure shows the majority (minority) states. States for complex wave vectors ($\kappa_z \neq 0$) are shown in the left ($q_z = 0$) and right ($q_z = \pi/a_{Fe}$) panel, the center panel shows bands with real wave vectors $\kappa_z = 0$. κ_z is given in absolute units of a.u.$^{-1}$ = 1.89 Å^{-1}. For an explanation of the line colors, see text.

form open parabolas. Some general complex bands plotted with pairs of yellow dots can be spotted, for example, the bands leaving the extrema of the complex bands with $q_z = 0$ (red) and connecting them with a small oval shaped ring (green) at $q_z = 1/2 \times \pi/a_{\mathrm{Cu}}$. Due to the finite energy mesh, very flat bands are hard to obtain as one can see for the band crossing the real bands at about -2.3 eV as indicated by the dashed line. Comparing the complex band structure with the results obtained in Refs. 6,45 one finds a good overall agreement. However, a closer inspection reveals some differences with the results of Krasovskii and Schattke[45] in the complex part of the band structure. In particular, differences can be found for the flat band at about -2.3 eV. In Fig. 3 of Ref. 45 this band has a minimum in the right panel while the present results as well as in the ones of Wachutka[6] show a very flat band up to $\kappa_z \sim 1.2$ a.u.$^{-1}$. For the same band a second difference is found in the left panel. While we and Wachutka[6] find three bands intersecting at $\kappa_z \sim 1.2$ a.u.$^{-1}$, this accidental degeneracy is not obtained by Krasovskii and Schattke.[45] As stated by these authors, the differences might be due to the overestimation of the dispersion of flat bands by the **kp** method used.

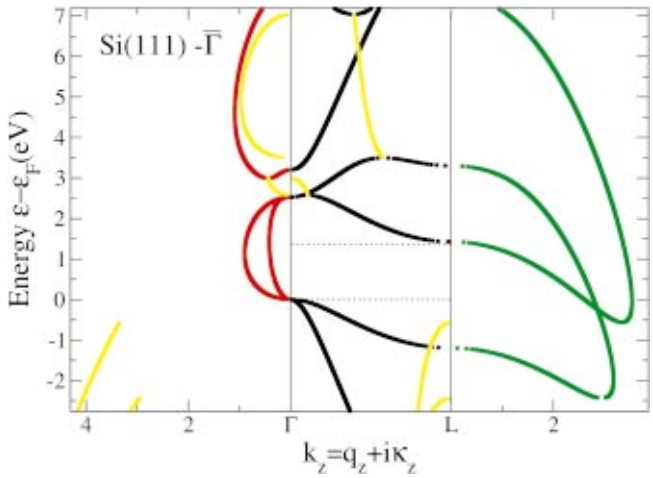

FIG. 6. (Color) Complex band structure of bulk Si for $\vec{k}_{\|}$ chosen at the $\bar{\Gamma}$ point of the two-dimensional Brillouin zone of an (111) oriented interface plane. States for complex wave vectors ($\kappa_z \neq 0$) are shown in the left ($q_z = 0$) and right ($q_z = \sqrt{3} \times \pi/a_{Si}$) panel ($a_{\mathrm{Si}} = 5.43$ Å), the center panel shows bands with real wave vectors $\kappa_z = 0$. κ_z is given in absolute units of a.u.$^{-1}$ = 1.89 Å^{-1}. Dotted lines indicate the indirect band gap along the Γ-L line. For an explanation of the line colors, see text.

B. Fe(001)-$\bar{\Gamma}$

As second example we present in Fig. 5 the complex band structure of ferromagnetic bulk Fe in the [001] direction, at the $\bar{\Gamma}$ point $\vec{k}_{\|} = (0,0)$ of the two-dimensional Brillouin zone. The q_z values follow the Δ line in the bulk Brillouin zone, connecting the Γ point and the H point, left and right high-symmetry points, respectively. Since Fe is a ferromagnet, the two spins are no longer degenerate and both a complex band structure for the majority and minority spin are displayed. The topology of the minority and majority bands is the same, but the energy positions of the bands are shifted by the exchange splitting. This affects largely the $3d$ bands and amounts to about 2.2 eV. The relatively flat real $3d$ bands in the energy range between -3 and 0 eV in the case of the majority spin are shifted to higher energy in the minority spin. At the Γ and X points the bands have either maxima and minima and continue dispersing on new branches as complex bands. A peculiarity can be seen at the complex band marked by the arrows. At around -1.2 eV (0.5 eV) for the majority (minority) spin this band shows a rapid change in slope in both, its real and complex part. This might

be due to some interaction between the states of this band and the very flat real and complex bands near the Γ point of the Brillouin zone at the same energy.

C. Si(111)-$\bar{\Gamma}$

As the last example we consider Si in a diamond structure. It is chosen as an example of semiconductors and also as a system containing more than one atom in a bulk unitcell. Differently from the former two examples, we calculate the complex bands in the [111] direction. Perpendicular to this direction, the Si atomic planes are stacked with two alternating interlayer spacings, where the larger distance corresponds to the nearest-neighbor Si-Si bond length. If one chooses the boundary surfaces S_L and S_R at the center of those neighboring Si planes bonded in the [111] direction, S_L and S_R do not cut any muffin-tin spheres of Si atoms. This signifies that the present system belongs to one of the exceptional cases where one does not need to introduce extra auxiliary regions Δ_L and Δ_R. It may be studied easily also by previous LAPW-based methods[7] having no prescription for treating the overlap of muffin-tin spheres in the surface normal direction.

In Fig. 6 we show the calculated complex band structure of Si in the [111] direction at the $\bar{\Gamma}$ point ($\vec{k}_\parallel = 0$), where the energy is measured relative to the valence-band maximum. The q_z values follow the Λ line in the bulk Brillouin zone, connecting the Γ point and the L point, left and right high-symmetry points, respectively. The calculated minimum energy difference between the conduction and valence bands along the Γ-L line amounts to 1.4 eV, which reproduces a typical LDA value for Si. Our calculation reproduces the well-known real energy-band dispersions of Si along the Γ-L line. At both ends of this line, these bands take either maximum or minimum values and evolve as new branches that disperse within the κ_z-ϵ plane. There also appear general complex bands with nonvanishing q_z and κ_z, which connect minima and maxima of the real and imaginary energy bands. Stiles and Hamann[7] studied the complex band structure of Si in the [111] direction using a wave-function method that relies upon the LAPW basis functions and a bivariational principle. Their complex band structure is in excellent agreement with ours in Fig. 6.

VII. SUMMARY

We presented a new flexible and widely applicable method to calculate the transfer matrix from first principles. The transfer matrix is expressed in terms of a single-electron Green function that fulfills an arbitrary boundary condition on both sides of the slab. We have shown that a particularly simple form can be obtained by imposing the von Neumann boundary condition. The Green function satisfying this condition is constructed by making use of the embedding theory of Inglesfield. The formulation allows us to describe systems with arbitrary boundary conditions making the formulation of wavefunction matching possible. We expanded the Green function and the transfer matrix in the LAPW basis of the FLAPW method. This guarantees a precise and flexible method, applicable to almost any system with two-dimensional translation symmetry including magnetic materials and systems with open structures.

The applicability of this new method has been demonstrated determining the complex band structures of bulk Cu, Fe, and Si. The results are in excellent agreement with the ones existing in the literature. Future applications of more intrinsic interest for the magneto-electronics may include half-metallics and oxide barrier materials for tunnel magnetoresistance devices.

So far the calculation of the transfer matrix relies on the assumption that the potential of the region of interest can be determined in some slab and supercell geometry. The transfer matrix opens the perspective to study semi-infinite systems or systems with internal interfaces separating semi-infinite half spaces, by taking into account self-consistently the surface or interface induced changes of the potential and charge density. As we have shown this may become possible either using the transfer matrix to obtain the embedding potential necessary to embed a surface or interface region by a Green-function method or use wave function matching. The wave function matching introduced for the calculation of transmission coefficients also enables the calculation of the corresponding boundary values of the states extended throughout all space. The boundary values together with Eq. (4) govern the wave function of the embedded system and consequently also the charge density and potential. In the future we may also invoke the linear scaling algorithm inherently available in the *T*-matrix method. Region Ω would be split up into smaller subregions Ω_i, the transfer matrix T_i is calculated for each subregion, and the total transfer matrix is obtained by successive application of the T_i's, $T = \Pi_i T_i$. Such a method would scale linear in the number of layers in Ω and thus could make the treatment of large systems accessible.

ACKNOWLEDGMENTS

We thank G. Bihlmayer for valuable help. D.W. thanks the DAAD and the HGF-Strategiefonds ''Magnetoelectronics'' for financial support. H.I. thanks the Alexander von Humboldt foundation for support during his stay in Jülich.

APPENDIX

As described in Sec. II the calculation of the *T* matrix does not require the use of a special Green function. In general the *T* matrix is given by

$$T = \begin{pmatrix} T_{11} & T_{12} \\ T_{21} & T_{22} \end{pmatrix}. \tag{A1}$$

The submatrices T_{11}, T_{12}, T_{21}, and T_{22} are given by the following set of equations:

$$T_{11}=\frac{1}{A}(-G_{LR}^{-1}\partial_n G_{LL}+2G_{LR}^{-1}+G_{RR}^{-1}\partial_n G_{RL}), \quad \text{(A2)}$$

$$T_{12}=\frac{1}{A}(G_{LR}^{-1}G_{LL}-G_{RR}^{-1}G_{RL}), \quad \text{(A3)}$$

$$T_{21}=-2G_{LR}^{-1}+G_{LR}^{-1}\partial_n G_{LL}+G_{LR}^{-1}\partial_n G_{LR}T_{11}, \quad \text{(A4)}$$

$$T_{22}=-G_{LR}^{-1}G_{LL}+G_{LR}^{-1}\partial_n G_{LR}T_{12}, \quad \text{(A5)}$$

with

$$A=-G_{RR}^{-1}\partial_n G_{RR}+2G_{RR}^{-1}+G_{LR}^{-1}\partial_n G_{LR}. \quad \text{(A6)}$$

*Electronic address: d.wortmann@fz-juelich.de

[1] J. A. Appelbaum and D. R. Hamann, Phys. Rev. B **6**, 2166 (1972).
[2] K. Hirose and M. Tsukada, Phys. Rev. Lett. **73**, 150 (1994).
[3] K. Hirose and M. Tsukada, Phys. Rev. B **51**, 5278 (1995).
[4] A. Nakamura, M. Brandbyge, L. B. Hansen, and K. W. Jacobsen, Phys. Rev. Lett. **82**, 1538 (1999).
[5] N. Kobayashi, M. Brandbyge, and M. Tsukada, Phys. Rev. B **62**, 8430 (2000).
[6] G. Wachutka, Phys. Rev. B **34**, 8512 (1986).
[7] M. D. Stiles and D. R. Hamann, Phys. Rev. B **38**, 2021 (1988).
[8] M. D. Stiles, J. Appl. Phys. **79**, 5805 (1996).
[9] N. D. Lang, Phys. Rev. B **52**, 5335 (1995).
[10] M. Di Ventra, S. T. Pantelides, and N. D. Lang, Phys. Rev. Lett. **84**, 979 (2000).
[11] M. Di Ventra, S.-G. Kim, S. T. Pantelides, and N. D. Lang, Phys. Rev. Lett. **86**, 288 (2001).
[12] J. van Hoof, K. Schep, P. Kelly, and G. Bauer, J. Magn. Magn. Mater. **177-181**, 188 (1998).
[13] J. E. Inglesfield, J. Phys. C **14**, 3795 (1981).
[14] M. Büttiker, Phys. Rev. Lett. **57**, 1761 (1986).
[15] R. Naaman, A. Haran, A. Nitzan, D. Evans, and M. Galperin, J. Phys. Chem. B **102**, 3658 (1998).
[16] P. Sautet and C. Joachim, Phys. Rev. B **38**, 12 238 (1988).
[17] J. Ferrer, A. Martin-Rodero, and F. Flores, Phys. Rev. B **38**, 10 113 (1988).
[18] L. Chico, L. X. Benedict, S. G. Louie, and M. L. Cohen, Phys. Rev. B **54**, 2600 (1996).
[19] J. Cerdá, M. A. Van Hove, P. Sautet, and M. Salmeron, Phys. Rev. B **56**, 15 885 (1997).
[20] J. Mathon, Phys. Rev. B **56**, 11 810 (1997).
[21] J. Kudrnovský, V. Drchal, C. Blaas, P. Weinberger, I. Turek, and P. Bruno, Phys. Rev. B **62**, 15 084 (2000).
[22] K. Xia, P. Kelly, G. Bauer, I. Turek, J. Kudrnovský, and V. Drchal, Phys. Rev. B **63**, 064407 (2001).
[23] N. Kar and P. Soven, Solid State Commun. **19**, 1041 (1976).
[24] K. Wildberger, R. Zeller, P. H. Dederichs, J. Kudrnovsky, and P. Weinberger, Phys. Rev. B **58**, 13 721 (1998).
[25] I. Riedel, P. Zahn, and I. Mertig, Phys. Rev. B **63**, 195403 (2001).
[26] H.-S. Sim, H.-W. Lee, and K. J. Chang, Phys. Rev. Lett. **87**, 096803 (2001).
[27] P. Mavropoulos, N. Papanikolaou, and P. H. Dederichs, Phys. Rev. Lett. **85**, 1088 (2000).
[28] W. Kohn, Phys. Rev. **115**, 809 (1959).
[29] V. Heine, Surf. Sci. **2**, 1 (1964).
[30] H. Ishida and M. I. Trioni, Phys. Rev. B **63**, 155108 (2001).
[31] J. Inglesfield and G. Benesh, Phys. Rev. B **37**, 6682 (1988).
[32] S. Crampin, J. B. A. N. van Hoof, M. Nekovee, and J. E. Inglesfield, J. Phys.: Condens. Matter **4**, 1475 (1992).
[33] S. Crampin, M. Nekovee, J. B. A. N. van Hoof, and J. E. Inglesfield, Surf. Sci. **287/88**, 732 (1993).
[34] M. I. Trioni, G. P. Brivio, S. Crampin, and J. E. Inglesfield, Phys. Rev. B **53**, 8052 (1996).
[35] J. B. Pendry, *Low Energy Electron Diffraction* (Academic, London, 1974).
[36] H. Ishida, Surf. Sci. **388**, 71 (1997).
[37] E. E. Krasovskii, F. Starrost, and W. Schattke, Phys. Rev. B **59**, 10 504 (1999).
[38] H. Ishida, Phys. Rev. B **63**, 165409 (2001).
[39] D. Singh, Phys. Rev. B **43**, 6388 (1991).
[40] E. E. Krasovskii, A. N. Yaresko, and V. N. Antonov, J. Electron Spectrosc. Relat. Phenom. **68**, 157 (1994).
[41] E. E. Krasovskii, Phys. Rev. B **56**, 12 866 (1997).
[42] E. Sjöstedt, L. Nordström, and D. J. Singh, Solid State Commun. **114**, 15 (2000).
[43] J. M. Soler and A. R. Williams, Phys. Rev. B **40**, 1560 (1989).
[44] Y.-C. Chang, Phys. Rev. B **25**, 605 (1982).
[45] E. E. Krasovskii and W. Schattke, Solid State Commun. **93**, 775 (1995).